



FACULTAD DE CIENCIAS
UNIVERSIDAD DE CANTABRIA

**Search for dark matter production in
association with top quarks in the
dilepton final state at $\sqrt{s} = 13$ TeV**

A thesis submitted in fulfillment of the requirements for the
Degree of Doctor of Philosophy

Written by
Cédric Prieëls

Under the supervision of
**Jónatan Piedra Gómez
Pablo Martínez Ruiz del Árbol**

Santander, June 2020

Abstract

Resumen

Acknowledgments

Acronyms used

SM Standard Model	NFW Navarro-Frenk-White
DM Dark Matter	LAT Fermi Large Telescope
LHC Large Hadron Collider	IACT Imaging Atmospheric Cherenkov Telescopes
CMS Compact Muon Solenoid	CTA Cherenkov Telescope Array
ATLAS A Toroidal LHC ApparatuS	AMS Alpha Magnetic Spectrometer
CERN European Council for Nuclear Research	EFT Effective Field Theory
QFT Quantum Field Theory	ISR Initial State Radiation
CMB Cosmic Microwave Background	FSR Final State Radiation
ML Machine Learning	DMWG Dark Matter Working Group
MFV Minimal Flavour Violation	MET Missing Transverse Energy
WIMP Weakly Interactive Massive Particle	VBF Vector Boson Fusion
PF Particle Flow	BR Branching Ratio
BSM Beyond the Standard Model	LEP Large Electron Positron collider
MACHO Massive Compact Halo Object	ALICE A Large Ion Collider Experiment
MSSM Minimal Supersymmetric Standard Model	PS Proton Synchrotron
SI Spin Independent	SPS Super Proton Synchrotron
SD Spin Dependent	PU Pile Up
CL Confidence Level	PV Primary Vertex
QCD Quantum ChromoDynamics	ECAL Electromagnetic Calorimeter
ADMX Axion Dark Matter Experiment	HCAL Hadronic Calorimeter
CAST CERN Axion Solar Telescope	DT Drift tube
IAXO International Axion Observatory	CSC Cathode Strip Chamber
LNGS Laboratori Nazionali del Gran Sasso	RPC Resistive Plate Chamber
UED Universal Extra Dimensions	TIB/TBD Tracker Inner Barrel and Disks

TOB Tracker Outer Barrel

TEC Tracker EndCap

HO Hadron Outer

LS Long Shutdown

GEM Gas Electron Multiplier

L1 Level-1 Trigger

HLT High-Level Trigger

DAQ Data Acquisition System

DQM Data Quality Monitoring

DCS Detector Control System

WP Working Point

SC Super Cluster

KF Kalman Filter

GSF Gaussian Sum Filter

MVA Multi-Variate Analysis

CSV Combined Secondary Vertex

DNN Deep Neural Network

PUPPI Pileup Per Particle Identification

BW Breit-Wigner

MC Monte Carlo

UE Underlying Event

PDF Parton Density Function

LO Leading Order

NLO Next to Leading Order

MPI Multiple Parton Interaction

SF Scale Factors

AOD Analysis Object Data

EDM Event Data Model

DY Drell-Yan

DAS Data Aggregation System

Contents

1	Data, signals and backgrounds	1
1.1	The Monte Carlo (MC) simulation method	1
1.2	Files format	5
1.3	Analysis code	6
1.4	Data samples	6
1.5	Signal samples	7
1.6	Backgrounds prediction	7
1.6.1	Top production	7
1.6.2	Drell-Yan estimation	9
1.6.3	Non prompt contamination	9
1.6.4	$t\bar{t} + V$	10
1.6.5	Smaller backgrounds	10
1.6.6	Weights and corrections applied	10
2	Event selection	13
2.1	Objects selection	13
2.1.1	Triggers selection	13
2.1.2	Electron selection	13
2.1.3	Muon Working Point (WP)	13
2.1.4	Jet WP	13
2.2	Signal regions	13
2.3	Control regions	14
2.4	Background-signal discrimination	14
2.4.1	Discriminating variables	14
2.4.2	Neural network	15
3	Results and interpretations	17
3.1	Systematics and uncertainties	17

3.2 Results	17
4 Conclusions	19
4.1 Future prospects	19
Appendices	21
A Samples used	23
A.1 Data samples	23
A.2 Signal samples	23
A.3 Backgrounds samples	23
Bibliography	29

Chapter 1

Data, signals and backgrounds

In order to find a possible hint of the production of Dark Matter (DM) in the Large Hadron Collider (LHC) collisions considering our signal models of interest, briefly described in Section ??, the data collected needs to be compared with Monte Carlo (MC) simulations produced in a central way for each Standard Model (SM) process. Indeed, any deviation of the data observed with respect to what we expect to see, obtained from these MC simulations, might be the sign of some Beyond the Standard Model (BSM) physics. All of the steps needed to mathematically simulate the pp collisions of the LHC and to take into account the effect of the detector on the particles produced will first of all be introduced in Section 1.1.

Then, the different formats of files available to perform the analysis and the code used will be briefly introduced in Sections 1.2 and 1.3 and the different data samples collected during the Run II of operation of the LHC will be then detailed in Section 1.4, while the signal models and samples considered in this particular analysis along with the MC samples used for the simulation of the different backgrounds will be introduced in Sections 1.5 and 1.6 respectively.

1.1 The Monte Carlo (MC) simulation method

As previously explained, the generation of MC simulations for the most common SM processes is a crucial step of any analysis because they are considered to be the reference to which the data collected is compared in order to try and find some discrepancies, which could be the sign of the existence of BSM physics. Searches for exotic physics therefore heavily depend on these simulations, which need to be generated with great care and to which a large uncertainty is typically associated since the collision between the partons of two protons and the interaction between the particles produced and the detector itself are extremely complex by nature.

The basic idea of the MC simulation consists in using a random number generator to simulate the randomness of nature and produce as many events as computationally possible for all the SM processes, taking into account the probability density functions of these processes. This is performed by specific softwares called **event generators** and it is important to note that since we usually don't know everything about the SM or BSM process being generated, the perfect event generator does not exist.

To make the generation of such simulations a bit easier, the description of a typical pp collision can usually be divided into several steps that will now be described, as shown with the color code used in Figure 1.1. The typical approximations used to make this kind of simulation possible from the computational point of view will also be briefly introduced at this point.

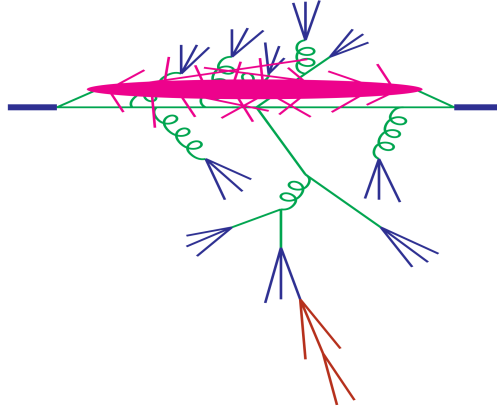


Figure 1.1: Structure of a pp collision and different steps of the MC simulation used by the event generators, such as the parton shower (in green), the UE (in pink), the hadronization (in blue) and the decay of unstable particles (in red) [101].

Hard scattering

A typical pp collision at a center of mass energy \sqrt{s} is usually described by an event generator as the interaction between a parton i coming from one proton with a parton j coming from the other, leading to the production of a final state A , made out of n different particles. The total cross section of such process can be expressed with Equation 1.1 [102].

$$\sigma_A(s) = \sum_{i,j} \int \int dx_1 dx_2 f_i(x_1, \mu^2) f_j(x_2, \mu^2) \hat{\sigma}_{ij \rightarrow A}(\hat{s}, \mu^2) \quad (1.1)$$

In this equation, several variables have been introduced, such as:

- The artificial parameter μ^2 used as the delimitation between short and long range physics.
- The Parton Density Functions (PDFs) $f_i(x, \mu^2)$ of both partons involved in the collision, giving the probability of finding in the proton a parton of flavor i (quark or gluon) carrying a fraction x of the proton momentum.
- The integrated parton-level cross section $\hat{\sigma}_{ij \rightarrow A}$ describing the short range physics between the partons, taking into account the phase space and the matrix element obtained considering all the Feynman diagrams of a given process.
- The square invariant mass of the two partons $\hat{s} = (p_i + p_j)^2$.

Many algorithms have been developed in order to select a hard process $ij \rightarrow A$ and determine its kinematics by solving this equation using different methods. The samples used in this work

have actually been produced at different orders and by different hard scattering generators, such as MADGRAPH [104] (at LO) and POWHEG [105] and MC@NLO [106] (at NLO).

Parton showers

The parton shower phase is then used to describe what happens to the incoming and outgoing partons after the initial collision that has just been described. The hard process induce by definition a large acceleration to the partons involved, which then tend to emit Quantum ChromoDynamics (QCD) radiation under the forms of gluons, just like accelerated electric charges do by emitting photons. However, the gluons emitted do have a color charge and can therefore emit further radiation until reaching such a low energy that they are able to form colourless hadrons, as discussed in Section ???. This process typically leads to the creation of the so-called **parton showers**, approximate higher-order real-emission corrections to the hard scattering, that need to be simulated by the event generators as well since they are an important part of the kinematics of the collision.

The parton showering then consists in simulating these showers for not only the final state particles produced by the hard scattering, but also for the particles in the initial state and for the remnants of the colliding protons, since gluons can actually be emitted by Initial State Radiation (ISR) and by these remnants themselves.

Underlying Event (UE)

Once the hard scattering and all the possible gluon emissions simulated, the next step consists in considering the so-called **Underlying Event (UE)** arising from the parton showers just described and from the secondary collisions between partons not involved in the primary hard process, the so-called Multiple Parton Interactions (MPIs). The UE is usually responsible for the production of particles at low transverse momenta p_T that cannot be experimentally distinguished from particles produced from initial or final state radiation but still need to be simulated.

These secondary collisions typically lead to the production of extra hadrons and therefore need to be simulated as well by events generators, usually by distributing the partons of the incoming protons in an area of 1fm^2 : an increased UE will be obtained when the so-called impact parameter, the distance between the parton and the centre of this area, is decreased, making the collision mostly central and almost head-on [107]. The UE is typically well simulated using softwares such as Herwig [108] and PYTHIA [109]. The spectrum for the generation of some variables in a top enriched sample can be found in Figure 1.2.

Hadronization

Once all the primary and secondary collisions simulated, it is time for the event generators to simulate the **hadronization** and binding processes of the different coloured partons emitted into colourless hadrons, as explained in Section ???. This hadronization process happen at low energies, when the perturbation theory becomes invalid and the dynamics enter a non-perturbative phase,

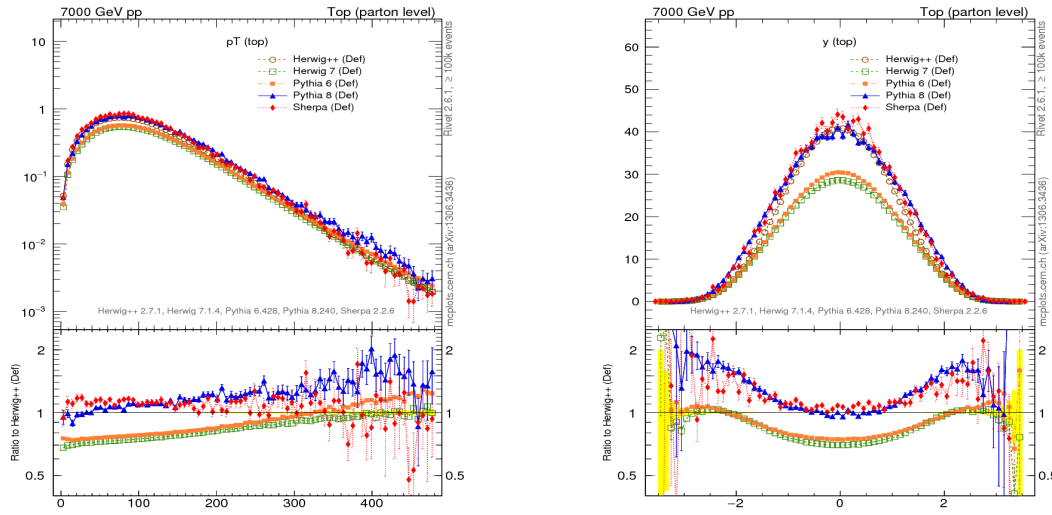


Figure 1.2: Top p_T (on the left) and rapidity (on the right) distributions obtained using different MC generators [110].

which leads to the formation of the observed final-state hadrons. Non-perturbative calculations then have to be used by the event generators in order to simulate this effect.

Unstable particle decays

The last step of the MC generation consists in finding a model allowing the unstable hadrons created in the hadronization process to decay, and to study these decays. This is extremely important because experimental data clearly shows that a large fraction of the observed final state particles come from the decays of such excited hadronic states.

Detector simulation

Once the event completely simulated using the event generators and the Pile Up (PU) taken into account by reproducing the hard scattering process several times, another step is required: simulating the interaction between the "perfect" particles previously created and the "imperfect" Compact Muon Solenoid (CMS) detector.

This is typically done by the GEANT4 software [111], able to model different effects, such as:

- Modeling of the interaction region
- Modeling of the particle passage through the volumes that compose CMS detector and of the accompanying physics processes
- Modeling of the effect of multiple interactions per beam crossing and/or the effect of events overlay (PU simulation)
- Modeling of the detector's electronics response

This modeling accounts for all the cracks and for the disposition of the subsystems inside of the CMS detector. This software is for example able to model the interaction of the electrons with the tracker, responsible for the emission of bremsstrahlung photons, as explained in Section ??.

The results of the comparison between the output of two different versions of the GEANT4 software and prototypes of the CMS calorimeter in the test beam facility at European Council for Nuclear Research (CERN) lead to comparable results, as shown in Figure 1.3.

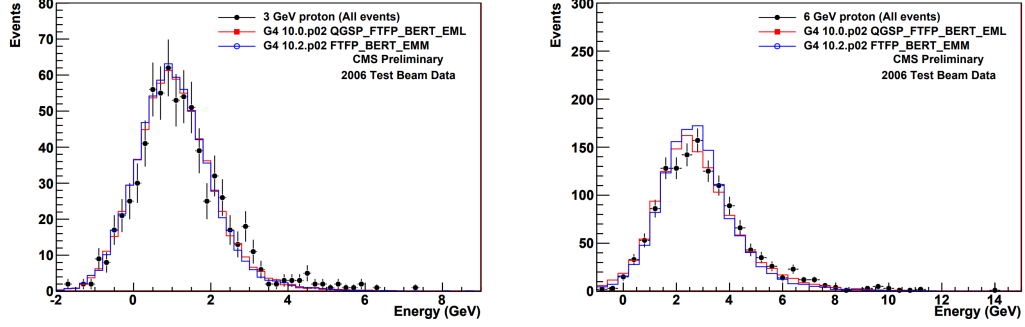


Figure 1.3: Proton energy distribution at 3 (on the left) and 6 (on the right) GeV compared for the test beam data (in black) and two different GEANT4 versions [112].

However, the modeling of the detector is not perfect and not all the inefficiencies can be accounted for. In some cases, Scale Factors (SF) are then used to correct the MC simulations and correct some expected discrepancies between data and MC. This will be detailed later on.

1.2 Files format

Once recorded (or simulated), the data (or MC) still needs to go under a complete post-processing in order to change its format and reduce the total size of the samples to be considered in the analyses. Different types of analysis are expected to need different levels of data reduction, so the data is usually accessible at different levels [113]:

- Virgin-RAW: used only in low rate runs with heavy ions collisions (10-15Mb/event)
- RAW : standard raw data event content (1Mb/event)
- RECO: detailed information on reconstructed physics objects (3Mb/event)
- Analysis Object Data (AOD): physics objects used in analysis (400-500kB/event)

Two additional formats were introduced since the end of the Run I. First of all the MiniAOD was introduced to reduce the size of the AOD by a factor 10 while retaining most of the information about all the particles that were created, without applying any further selection.

Because of the increased integrated luminosity collected by CMS over the last few years, a brand new file format featuring another reduction of the file size of a factor ~ 50 was recently introduced:

the nanoAOD, able to retain most of the information of each collision in around 1kB of data per event only. This reduction in size was achieved by optimizing the floating point of the variables, by not storing quantities that can be recomputed from the available information and by limiting the number of physics objects available, for example. This means that some low-level analyses cannot use this format to work, but it has been estimated that around 50-70% of the analyses performed at CMS can rely on such files in order to work.

In this particular case, the 6th version of the nanoAOD, introducing a series of bug fixes and the latest jet energy corrections, was used for both the data and the MC samples (signal and backgrounds) that will now be listed in the next sections.

1.3 Analysis code

The code used for the event generation, simulation and reconstruction is the version 10.2.X of the official software of the CMS collaboration, called CMSSW [115]. This software contains the CMS Event Data Model (EDM) which is able to describe every event as a C++ object containing all the RAW and reconstructed information related to the collision. These object are stored using the ROOT file format [116], an analysis package written in C++.

Once all the different samples produced centrally up to the nanoAOD stage, another framework was put in place in order to do a post-processing of such samples, by selecting objects interesting for different dileptonic analyses, reducing therefore even more the size of the samples to be considered by selecting only events having 2 tight leptons. This selection will be detailed in Chapter 2. This *Latino* framework, written in phyton, is common to several different analyses and has been developed by tens of different people over the past few years, providing several tools to produce samples, read the files, apply different corrections to the MC samples and produce the histograms needed to perform a search such as this one.

1.4 Data samples

As already explained in Section ??, the data analyzed in this work has been taken at a center of mass energy of 13 TeV during the second part of the Run II of operation of the LHC.

During this period, an integrated luminosity of $35.9 \pm 0.9 \text{ fb}^{-1}$ (2016) [117], $41.5 \pm 1.0 \text{ fb}^{-1}$ (2017) [118] and $59.7 \pm 1.5 \text{ fb}^{-1}$ (2018) [119] has been collected, resulting in a total dataset of $137.1 \pm 2.0 \text{ fb}^{-1}$ recorded by the CMS detector and ready to be analyzed. This data has been obtained by combining a set of single and double lepton triggers that will be described in Section 2.1.1 by taking care of avoiding any eventual double counting due to events present in different triggers. All the data samples considered for this analysis are listed in Section A.1.

1.5 Signal samples

To be completed once the files are actually available Listed in Section A.2.

1.6 Backgrounds prediction

Several different SM background processes have been considered for this analysis, all listed in Section A.3 and mostly estimated directly from MC. In this section, the main backgrounds to consider for this particular analysis will be quoted, such as:

- The major background for the $t\bar{t}$ +DM analysis is the SM $t\bar{t}$, kinematically close to the signal searched for (Section 1.6.1).
- On the other hand, the major background for the t/\bar{t} analysis is the single top production, which has an even higher cross section than the $t\bar{t}$ (Section 1.6.1).
- Then, mainly because of its huge cross section shown in Figure 1.4, the Drell-Yan (DY) process is usually quite important, even in the signal regions (Section 1.6.2).
- The non-prompt background, or fakes, is another important piece of this analysis mainly because of the particular data-driven method used to compute them (Section 1.6.3).
- Finally, the $t\bar{t} + V$ ($t\bar{t} + Z$ and $t\bar{t} + W$) may have a kinematics even closer to our signal than the $t\bar{t}$ process and is therefore extremely important in our signal regions, even though its low cross section does limit its impact (Section 1.6.4).

Add percentage of each background once known

Finally, some smaller backgrounds will be introduced in Section 1.6.5 and the weights and corrections applied to all these MC samples will be detailed in Section 1.6.6.

TALK ABOUT SINGLE TOP?

1.6.1 Top production

Dominant in both searches

The main background: $t\bar{t}$

This background is the most relevant for this analysis because of its large cross section (as seen in Appendix A, it is actually between ~ 4 and ~ 250.000 times larger than the expected cross section of our signal, depending on the mass point considered!) and kinematics quite close to the expected one for our signal when consider the possible decay of the top quarks into two leptons.

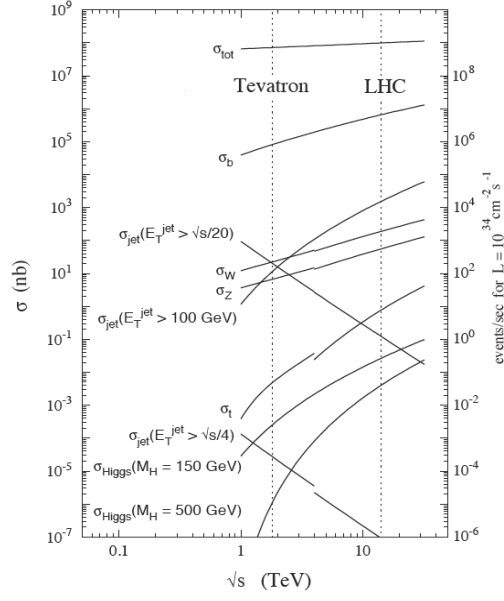


Figure 1.4: Production cross section of the most common SM processes considering different center of mass energies, such as the 13 TeV of the LHC.

Different Feynman diagrams contribute to this process at Leading Order (LO), as shown in Figure 1.5.

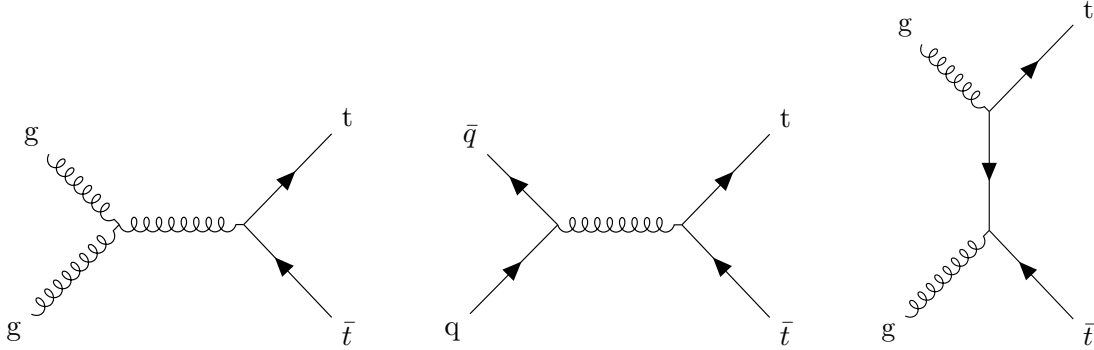


Figure 1.5: Main feynman diagrams for the production of the SM $t\bar{t}$ process.

This background is so similar to the signal searched for that some Machine Learning (ML) techniques had to be developed in order to find some discrimination between the two processes.

Single top

s-channel in Figure 1.6 other in Figure 1.7

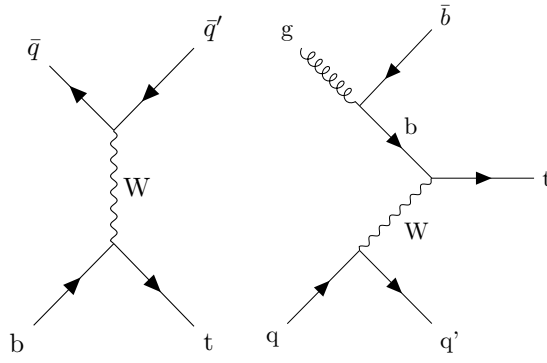


Figure 1.6: Feynman diagrams for s-channel production mode of a single top quarks.

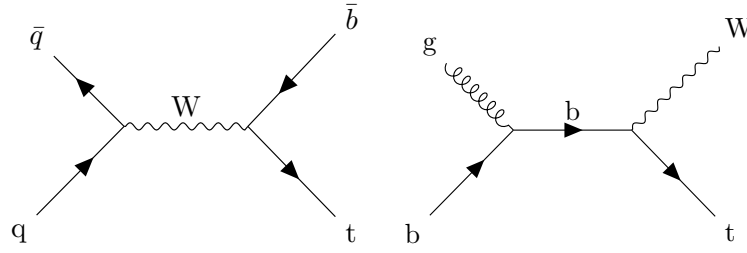


Figure 1.7: Feynman diagrams for t-channel (on the left) and tW (on the right) production modes of a single top quarks.

Top decay

1.6.2 Drell-Yan estimation

Figure 1.9.

1.6.3 Non prompt contamination

qcd? w+jets and z+jets in Figure 1.10

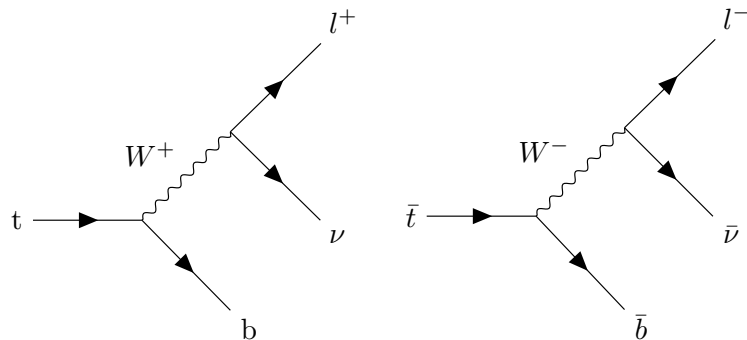


Figure 1.8: Feynman diagrams for the leptonic decay of the top (on the left) and antitop (on the right) quarks.

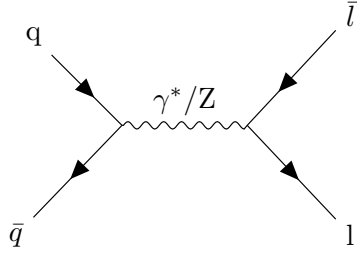


Figure 1.9: Feynman diagram for the DY process involving a virtual γ^* or Z boson.

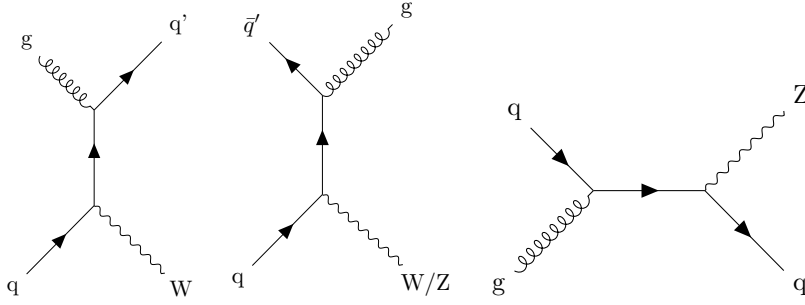


Figure 1.10: Possible Feynman diagrams for the production of a W/Z boson in association with a jet.

1.6.4 $t\bar{t} + V$

Figure 1.11

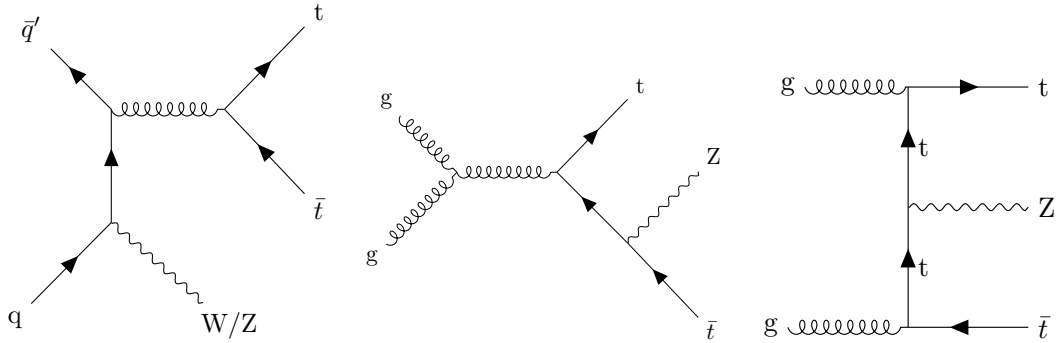


Figure 1.11: Possible Feynman diagrams for the Initial State Radiation (ISR) $t\bar{t}$ with a W/Z boson (on the left) and for the production of an Final State Radiation (FSR) $t\bar{t}Z$ (on the center and right).

1.6.5 Smaller backgrounds

Diboson contamination Figure 1.12.

1.6.6 Weights and corrections applied

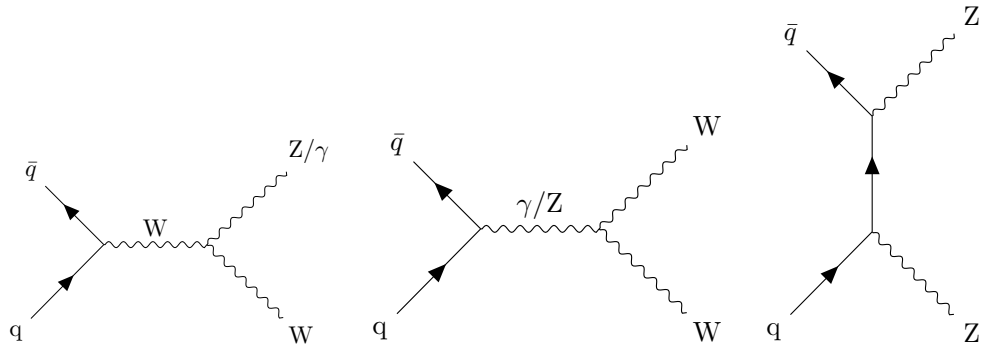


Figure 1.12: Possible Feynman diagrams for smaller backgrounds of this analysis: WW (on the left), $W\gamma$ and WZ (on the center) and ZZ (on the right).

Chapter 2

Event selection

2.1 Objects selection

2.1.1 Triggers selection

2.1.2 Electron selection

2.1.3 Muon WP

2.1.4 Jet WP

2.2 Signal regions

It is important to note that a strict **blinding policy** has been followed for this search, in order to avoid optimizing the analysis based on what has already seen. The data available to be plotted in the following signal regions has therefore been limited to 1 fb^{-1} for each year.

2.3 Control regions

2.4 Background-signal discrimination

2.4.1 Discriminating variables

Missing Transverse Energy (MET)

This variable has already been defined in Section ??, and corresponds to the imbalance in transverse momentum which can be left by different phenomena, such as the apparition of a SM neutrino or the existence of DM particles, able to escape the detector without being detected.

This variable is expected to induce some discrimination between the signal and the backgrounds because, even though the $t\bar{t}$ in the dilepton final state is expected to produce two neutrinos and therefore some MET, the $t\bar{t}$ +DM signal model is expected to have mostly the same contribution to the MET from its own two neutrinos, and an additional contribution from the pair $\chi\bar{\chi}$ produced. The MET spectrum is therefore expected to reach higher values for the signal than the backgrounds.

TALK ABOUT SINGLE TOP?

Stransverse mass

The m_{T2} variable, also called **stransverse mass**, is an extension of the definition of the transverse mass m_T to cases when pairs of particles with the same flavor decay into one visible and one invisible particle, such as what happens in the $W \rightarrow l\nu$ decay, for example.

In this particular case, two particles contribute to the presence of Missing Transverse Energy (MET) and the individual contribution of each particle (\not{p}_{T1} and \not{p}_{T2}) to this missing energy cannot be inferred. The stransverse mass is then defined according to Equation 2.1, where $\mathbf{p}_{Ti} = \vec{p}_{Ti}$ is the (visible) transverse momentum of the particle i and α is the angle between the visible and invisible p_T of the decay considered [114].

$$\begin{cases} M_{T2}^2 = \min_{\not{p}_{T1} + \not{p}_{T2} = \not{p}_{T_{\text{tot}}}} \left(\max \left(m_T^2(\mathbf{p}_{T1}, \not{p}_{T1}), m_T^2(\mathbf{p}_{T2}, \not{p}_{T2}) \right) \right) \\ m_T^2(\mathbf{p}_T, \not{p}_T) = 4 |\mathbf{p}_T| |\not{p}_T| \sin^2 \left(\frac{\alpha}{2} \right) \end{cases} \quad (2.1)$$

This equation can be understood in the following way: to compute the m_{T2} variable, different combinations ($\not{p}_{T1}, \not{p}_{T2}$) satisfying the condition $\not{p}_{T1} + \not{p}_{T2} = \not{p}_{T_{\text{tot}}}$ need to be probed, keeping only the combination which results in the lowest value.

In this particular analysis, $M_{T2}(ll)$ is calculated, since the role of the visible particles is played by the two final state leptons. This variable is expected to introduce some discrimination because,

according to the definition just given, the $M_{T2}(ll)$ variable for a SM $t\bar{t}$ process is expected to have an endpoint exactly at the mass of the W boson, while an eventual $t\bar{t}$ +DM signal does not have this limitation in the $M_{T2}(ll)$ spectrum because of the pair of DM particles produced, which also contributes to the total MET of the event.

However, in practice, we do observe a tail in this spectrum even for SM $t\bar{t}$ without DM, because of the instrumental MET sometimes observed or the fact that some selected leptons are not actually prompt leptons but can be jets misidentified as leptons by the detector.

TALK ABOUT SINGLE TOP?

2.4.2 Neural network

Chapter 3

Results and interpretations

3.1 Systematics and uncertainties

3.2 Results

Chapter 4

Conclusions

4.1 Future prospects

Appendices

Appendix A

Samples used

A.1 Data samples

All the data samples considered for this analysis are listed in Tables A.1, A.2 and A.3. The luminosity of each dataset has been computed using the Brilcalc tool provided by CMS [120], while the number of generated events has been obtained using the CERN official Data Aggregation System (DAS).

A.2 Signal samples

To be completed once the files are actually available

A.3 Backgrounds samples

To be completed once the analysis actually performed LO/NLO Generator used

Dataset	Events (size)	\mathcal{L} [fb ⁻¹]
Run 2016B		
/DoubleEG/Run2016B_ver2-Nano1June2019_ver2-v1/NANOAOD	143073268 (99.4Gb)	5.8
/DoubleMuon/Run2016B_ver2-Nano1June2019_ver2-v1/NANOAOD	82535526 (53.2Gb)	
/MuonEG/Run2016B_ver2-Nano1June2019_ver2-v1/NANOAOD	32727796 (26.8Gb)	
/SingleElectron/Run2016B_ver2-Nano1June2019_ver2-v1/NANOAOD	246440440 (167.8Gb)	
/SingleMuon/Run2016B_ver2-Nano1June2019_ver2-v1/NANOAOD	158145722 (96.4Gb)	
Run 2016C		
/DoubleEG/Run2016C-Nano1June2019-v1/NANOAOD	47677856 (35.3Gb)	2.6
/DoubleMuon/Run2016C-Nano1June2019-v1/NANOAOD	27934629 (19.7Gb)	
/MuonEG/Run2016C-Nano1June2019-v1/NANOAOD	15405678 (12.8Gb)	
/SingleElectron/Run2016C-Nano1June2019-v1/NANOAOD	97259854 (69.3Gb)	
/SingleMuon/Run2016C-Nano1June2019-v1/NANOAOD	67441308 (42.4Gb)	
Run 2016D		
/DoubleEG/Run2016D-Nano1June2019-v1/NANOAOD	53324960 (39.6Gb)	4.2
/DoubleMuon/Run2016D-Nano1June2019-v1/NANOAOD	33861745 (24.1Gb)	
/MuonEG/Run2016D-Nano1June2019-v1/NANOAOD	23482352 (19.4Gb)	
/SingleElectron/Run2016D-Nano1June2019-v1/NANOAOD	148167727 (104.4Gb)	
/SingleMuon/Run2016D-Nano1June2019-v1/NANOAOD	98017996 (61.3Gb)	
Run 2016E		
/DoubleEG/Run2016E-Nano1June2019-v1/NANOAOD	49877710 (37.9Gb)	4.0
/DoubleMuon/Run2016E-Nano1June2019-v1/NANOAOD	28246946 (20.8Gb)	
/MuonEG/Run2016E-Nano1June2019-v2/NANOAOD	22519303 (19.0Gb)	
/SingleElectron/Run2016E-Nano1June2019-v1/NANOAOD	117321545 (86.5Gb)	
/SingleMuon/Run2016E-Nano1June2019-v1/NANOAOD	90984718 (58.7Gb)	
Run 2016F		
/DoubleEG/Run2016F-Nano1June2019-v1/NANOAOD	34577629 (26.9Gb)	3.1
/DoubleMuon/Run2016F-Nano1June2019-v1/NANOAOD	20329921 (15.3Gb)	
/MuonEG/Run2016F-Nano1June2019-v1/NANOAOD	16002165 (13.6Gb)	
/SingleElectron/Run2016F-Nano1June2019-v1/NANOAOD	70593532 (51.4Gb)	
/SingleMuon/Run2016F-Nano1June2019-v1/NANOAOD	65489554 (42.4Gb)	
Run 2016G		
/DoubleEG/Run2016G-Nano1June2019-v1/NANOAOD	78797031 (61.6Gb)	7.6
/DoubleMuon/Run2016G-Nano1June2019-v1/NANOAOD	45235604 (34.2Gb)	
/MuonEG/Run2016G-Nano1June2019-v1/NANOAOD	33854612 (29.0Gb)	
/SingleElectron/Run2016G-Nano1June2019-v1/NANOAOD	153363109 (109.2Gb)	
/SingleMuon/Run2016G-Nano1June2019-v1/NANOAOD	149912248 (94.6Gb)	
Run 2016H		
/DoubleEG/Run2016H-Nano1June2019-v1/NANOAOD	85388734 (67.7Gb)	8.6
/DoubleMuon/Run2016H-Nano1June2019-v1/NANOAOD	48912812 (37.3Gb)	
/MuonEG/Run2016H-Nano1June2019-v1/NANOAOD	29236516 (26.0Gb)	
/SingleElectron/Run2016H-Nano1June2019-v1/NANOAOD	128854598 (93.8Gb)	
/SingleMuon/Run2016H-Nano1June2019-v1/NANOAOD	174035164 (110.2Gb)	

Table A.1: Datasets collected in 2016 and considered for this analysis.

Dataset	Events (size)	\mathcal{L} [fb ⁻¹]
Run 2017B		
/DoubleEG/Run2017B-Nano1June2019-v1/NANOAOD	58088760 (46.6Gb)	4.8
/DoubleMuon/Run2017B-Nano1June2019-v1/NANOAOD	14501767 (10.8Gb)	
/SingleElectron/Run2017B-Nano1June2019-v1/NANOAOD	60537490 (42.2Gb)	
/SingleMuon/Run2017B-Nano1June2019-v1/NANOAOD	136300266 (86.2Gb)	
/MuonEG/Run2017B-Nano1June2019-v1/NANOAOD	4453465 (4.1Gb)	
Run 2017C		
/DoubleEG/Run2017C-Nano1June2019-v1/NANOAOD	65181125 (53.8Gb)	9.7
/DoubleMuon/Run2017C-Nano1June2019-v1/NANOAOD	49636525 (39.5Gb)	
/SingleElectron/Run2017C-Nano1June2019-v1/NANOAOD	136637888 (102.5Gb)	
/SingleMuon/Run2017C-Nano1June2019-v1/NANOAOD	165652756 (109.5Gb)	
/MuonEG/Run2017C-Nano1June2019-v1/NANOAOD	15595214 (15.0Gb)	
Run 2017D		
/DoubleEG/Run2017D-Nano1June2019-v1/NANOAOD	25911432 (21.6Gb)	4.2
/DoubleMuon/Run2017D-Nano1June2019-v1/NANOAOD	23075733 (18.6Gb)	
/SingleElectron/Run2017D-Nano1June2019-v1/NANOAOD	51526710 (38.5Gb)	
/SingleMuon/Run2017D-Nano1June2019-v1/NANOAOD	70361660 (47.2Gb)	
/MuonEG/Run2017D-Nano1June2019-v1/NANOAOD	9164365 (8.9Gb)	
Run 2017E		
/DoubleEG/Run2017E-Nano1June2019-v1/NANOAOD	56233597 (49.8Gb)	9.3
/DoubleMuon/Run2017E-Nano1June2019-v1/NANOAOD	51589091 (44.4Gb)	
/SingleElectron/Run2017E-Nano1June2019-v1/NANOAOD	102121689 (81.3Gb)	
/SingleMuon/Run2017E-Nano1June2019-v1/NANOAOD	154630534 (111.0Gb)	
/MuonEG/Run2017E-Nano1June2019-v1/NANOAOD	19043421 (19.2Gb)	
Run 2017F		
/DoubleEG/Run2017F-Nano1June2019-v1/NANOAOD	74307066 (67.1Gb)	13.5
/DoubleMuon/Run2017F-Nano1June2019-v1/NANOAOD	79756560 (68.0Gb)	
/SingleElectron/Run2017F-Nano1June2019-v1/NANOAOD	128467223 (105.2Gb)	
/SingleMuon/Run2017F-Nano1June2019-v1/NANOAOD	242135500 (178.3Gb)	
/MuonEG/Run2017F-Nano1June2019-v1/NANOAOD	25776363 (26.3Gb)	

Table A.2: Datasets collected in 2017 and considered for this analysis.

Dataset	Events (size)	\mathcal{L} [fb ⁻¹]
Run 2018A		
/DoubleMuon/Run2018A-Nano25Oct2019-v1/NANOAOD	75499908 (62.6Gb)	13.5
/EGamma/Run2018A-Nano25Oct2019-v1/NANOAOD	327843843 (261.8Gb)	
/SingleMuon/Run2018A-Nano25Oct2019-v1/NANOAOD	241608232 (167.7Gb)	
/MuonEG/Run2018A-Nano25Oct2019-v1/NANOAOD	32958503 (32.3Gb)	
Run 2018B		
/DoubleMuon/Run2018B-Nano25Oct2019-v1/NANOAOD	35057758 (28.3Gb)	6.8
/EGamma/Run2018B-Nano25Oct2019-v1/NANOAOD	153822427 (123.1Gb)	
/SingleMuon/Run2018B-Nano25Oct2019-v1/NANOAOD	119918017 (82.3Gb)	
/MuonEG/Run2018B-Nano25Oct2019-v1/NANOAOD	16211567 (15.8Gb)	
Run 2018C		
/DoubleMuon/Run2018C-Nano25Oct2019-v1/NANOAOD	34565869 (27.6Gb)	6.6
/EGamma/Run2018C-Nano25Oct2019-v1/NANOAOD	147827904 (119.2Gb)	
/SingleMuon/Run2018C-Nano25Oct2019-v1/NANOAOD	110032072 (75.7Gb)	
/MuonEG/Run2018C-Nano25Oct2019-v1/NANOAOD	15652198 (15.3Gb)	
Run 2018D		
/DoubleMuon/Run2018D-Nano25Oct2019_ver2-v1/NANOAOD	168605834 (128.6Gb)	32.0
/EGamma/Run2018D-Nano25Oct2019-v1/NANOAOD	751348648 (583.6Gb)	
/SingleMuon/Run2018D-Nano25Oct2019-v1/NANOAOD	513867253 (344.5Gb)	
/MuonEG/Run2018D-Nano25Oct2019_ver2-v1/NANOAOD	71961587 (68.6Gb)	

Table A.3: Datasets collected in 2018 and considered for this analysis.

List of figures

1.1	Structure of a pp collision and different steps of the MC simulation used by the event generators, such as the parton shower (in green), the UE (in pink), the hadronization (in blue) and the decay of unstable particles (in red) [101].	2
1.2	Top p_T (on the left) and rapidity (on the right) distributions obtained using different MC generators [110].	4
1.3	Proton energy distribution at 3 (on the left) and 6 (on the right) GeV compared for the test beam data (in black) and two different GEANT4 versions [112].	5
1.4	Production cross section of the most common SM processes considering different center of mass energies, such as the 13 TeV of the LHC.	8
1.5	Main feynman diagrams for the production of the SM $t\bar{t}$ process.	8
1.6	Feynman diagrams for s-channel production mode of a single top quarks.	9
1.7	Feynman diagrams for t-channel (on the left) and tW (on the right) production modes of a single top quarks.	9
1.8	Feynman diagrams for the leptonic decay of the top (on the left) and antitop (on the right) quarks.	9
1.9	Feynman diagram for the DY process involving a virtual γ^* or Z boson.	10
1.10	Possible Feynman diagrams for the production of a W/Z boson in association with a jet.	10
1.11	Possible Feynman diagrams for the Initial State Radiation (ISR) $t\bar{t}$ with a W/Z boson (on the left) and for the production of an Final State Radiation (FSR) $t\bar{t}Z$ (on the center and right).	10
1.12	Possible Feynman diagrams for smaller backgrounds of this analysis: WW (on the left), $W\gamma$ and WZ (on the center) and ZZ (on the right).	11

List of tables

A.1	Datasets collected in 2016 and considered for this analysis.	24
A.2	Datasets collected in 2017 and considered for this analysis.	25
A.3	Datasets collected in 2018 and considered for this analysis.	26

Bibliography

- [1] F. Englert and R. Brout, "Broken symmetry and the mass of gauge vector mesons", Phys. Rev. Lett. 13, pp. 321-323, 1964
- [2] P. W. Higgs, "Broken symmetries and the masses of gauge bosons", Phys. Rev. Lett. 13, pp. 508-509, 1964
- [3] S. Chatrchyan et al., "Observation of a new boson at a mass of 125 GeV with the CMS experiment at the LHC", Phys. Lett. B716, pp. 30-61, 2012 [arXiv: 1207.7235]
- [4] G. Aad et al., "Observation of a new particle in the search for the Standard Model Higgs boson with the ATLAS detector at the LHC", Phys. Lett. B716, pp. 1-29, 2012 [arXiv: 1207.7214]
- [5] V.C. Rubin, W.K. Ford and N. Thonnard, "Rotational properties of 21 SC galaxies with a large range of luminosities and radii, from NGC 4605 (R=4kpc) to UGC 2885 (R=122kpc)", Astrophysical Journal 238, pp. 471-487, 1980
- [6] K.G. Begeman, A.H. Broeils and R.H. Sanders, "Extended rotation curves of spiral galaxies - Dark haloes and modified dynamics", Monthly Notices of the Royal Astronomical Society, vol. 249, issue 3, ISSN 0035-8711, 1991
- [7] A. Robertson, R. Massey and V. Eke, "What does the Bullet Cluster tell us about self-interacting dark matter?", Monthly Notices of the Royal Astronomical Society, vol. 465, issue 1, 2017 [arXiv: 1605.04307]
- [8] J.B. Muñoz, C. Dvorkin and A. Loeb, "21-cm Fluctuations from Charged Dark Matter", Phys. Rev. Lett. 121, 121301 (2018) [arXiv: 1804.01092]
- [9] A. Natarajan, "A closer look at CMB constraints on WIMP dark matter", Phys. Rev. D85, 2012 [arXiv:1201.3939]
- [10] G. D'Ambrosio, G.F. Giudice, G. Isidori and A. Strumia, "Minimal Flavour Violation: an effective field theory approach", Nucl.Phys. 645, pp 155-187, 2002 [arXiv:0207.036]
- [11] CMS Collaboration, "Search for the production of dark matter in association with top-quark pairs in the single-lepton final state in proton-proton collisions at $\sqrt{s} = 8$ TeV", JHEP, vol. 6 121, 2015
- [12] CMS Collaboration, "Search for the Production of Dark Matter in Association with Top Quark Pairs in the Di-lepton Final State in pp collisions at $\sqrt{s} = 8$ TeV", CMS-PAS-B2G-13-004, 2014

- [13] "Search for dark matter in events with heavy quarks and missing transverse momentum in pp collisions with the ATLAS detector", Eur. Phys. J. C (2015) 75:92
- [14] ATLAS Collaboration, Search for the Supersymmetric Partner of the Top Quark in the Jets+Emiss Final State at $\sqrt{s} = 13$ TeV", ATLAS-CONF-2016-077
- [15] ATLAS Collaboration, "Search for top squarks in final states with one isolated lepton, jets, and missing transverse momentum in $\sqrt{s} = 13$ TeV pp collisions with the ATLAS detector", ATLAS-CONF-2016-050, 2016
- [16] ATLAS Collaboration, "Search for direct top squark pair production and dark matter production in final states with two leptons in $\sqrt{s} = 13$ TeV pp collisions using 13.3 fb^{-1} of ATLAS data", ATLAS-CONF-2016-076, 2016
- [17] ATLAS Collaboration, "Search for dark matter produced in association with bottom or top quarks in $\sqrt{s} = 13$ TeV pp collisions with the ATLAS detector", Eur. Phys. J. C 78 (2018) 18 [arXiv: 1710.11412]
- [18] CMS Collaboration, Search for dark matter produced in association with heavy-flavor quark pairs in proton-proton collisions at $\sqrt{s} = 13$ TeV", Eur. Phys. J. C (2017) 77: 845
- [19] CMS Collaboration, "Search for dark matter particles produced in association with a top quark pair at $\sqrt{s} = 13$ TeV", Phys. Rev. Lett. 122, 011803 (2019) [arXiv: 1807.06522]
- [20] CMS Collaboration, "Search for dark matter produced in association with a single top quark or a top quark pair in proton-proton collisions at $\sqrt{s} = 13$ TeV", JHEP, vol. 03 141, 2019 [arXiv: 1901.01553]
- [21] S. Manzoni, "The Standard Model and the Higgs Boson", Physics with Photons Using the ATLAS Run 2 Data, Springer Theses, 2019
- [22] A.B. Balantekin, A. Gouvea and B.Kayser, "Addressing the Majorana vs. Dirac Question with Neutrino Decays", FERMILAB-PUB-18-418-T, NUHEP-TH/18-09 [arXiv: 1808.10518]
- [23] J. Woithe, G.J. Wiener and F. Van der Vecken, "Let's have a coffee with the Standard Model of particle physics!", Physics education 52, number 3, 2017
- [24] F. Zwicky, "Die Rotverschiebung von extragalaktischen Nebeln", Helvetica Physica Acta , vol. 6, pp. 110-127, 1933
- [25] S. Van den Bergh, Phys Rev D "The early history of dark matter", Dominion Astrophysical Observatory, 1999
- [26] V.C. Rubin, W.K. Ford, "Rotation of the Andromeda Nebula from a Spectroscopic Survey of Emission Regions", Astrophysical Journal 159, p. 379, 1970
- [27] A. A. Penzias, R.W. Wilson, "A Measurement of Excess Antenna Temperature at 4080 Mc/s", Astrophysical Journal 142, pp. 419-421
- [28] D.J. Fixsen, "The temperature of the cosmic microwave background", Astrophysical Journal, 2009

- [29] Planck Collaboration, "Planck 2018 results. I. Overview and the cosmological legacy of Planck", 2018 [arXiv: 1807.06205]
- [30] R. Tojeiro, "Understanding the Cosmic Microwave Background Temperature Power Spectrum", 2006
- [31] Planck Collaboration, "Planck 2018 results. VI. Cosmological parameters", 2018 [arXiv: 1807.06209]
- [32] "Astrophysical Constants and Parameters", 2019
- [33] D. Clowe et al., "A Direct Empirical Proof of the Existence of Dark Matter", *Astrophysical Journal Letters* 648, 2006
- [34] K.R. Dienes, J. Fennick, J. Kumar, B. Thomas "Dynamical Dark Matter from Thermal Freeze-Out", *Phys. Rev. D* 97, 063522 (2018) [arXiv: 1712.09919]
- [35] C.S. Frenk, S.D.M. White, "Dark matter and cosmic structure", *Annalen der Physik*, p. 22 , 2012 [arXiv: 1210.0544]
- [36] R. Kirk, "Dark matter genesis"
- [37] M. Drewes et al., "A White Paper on keV Sterile Neutrino Dark Matter", 2016 [arXiv: 1602.04816]
- [38] C. Alcock et al., "The MACHO Project: Microlensing Results from 5.7 Years of LMC Observations", *Astrophys.J.* 542 (2000) 281-307
- [39] P. Tisserand et al., "Limits on the Macho content of the Galactic Halo from the EROS-2 Survey of the Magellanic Clouds", *A & A* 469, pp. 387-404 (2007)
- [40] EROS and MACHO collaborations, "EROS and MACHO Combined Limits on Planetary Mass Dark Matter in the Galactic Halo", 1998
- [41] Particle Data Group, "Neutrino Cross Section Measurements", PDG 2019
- [42] K. McFarland, "Neutrino Interactions", 2008 [arXiv: 0804.3899]
- [43] E. Morgante, "Aspects of WIMP Dark Matter Searches at Colliders and Other Probes", Springer theses, 2016
- [44] F. Couchot et al., "Cosmological constraints on the neutrino mass including systematic uncertainties", *A & A* 606, A104 (2017)
- [45] E. Bulbul et al., "Detection of An Unidentified Emission Line in the Stacked X-ray spectrum of Galaxy Clusters", 2014 [arXiv: 1402.2301]
- [46] A. Boyarsky et al., "An unidentified line in X-ray spectra of the Andromeda galaxy and Perseus galaxy cluster", *Phys. Rev. Lett.* 113, 251301 (2014) [arXiv: 1402.4119]
- [47] A. Boyarsky et al., "Checking the dark matter origin of 3.53 keV line with the Milky Way center", *Phys. Rev. Lett.* 115, 161301 (2015) [arXiv: 1408.2503]

- [48] T. Jeltema and S. Profumo, "Deep XMM Observations of Draco rule out at the 99% Confidence Level a Dark Matter Decay Origin for the 3.5 keV Line", 2015 [arXiv: 1512.01239]
- [49] D. Wu, "A Brief Introduction to the Strong CP Problem", Superconducting Super Collider Laboratory, 1991
- [50] R.D. Peccei, H.R. Quinn, "CP Conservation in the Presence of Pseudoparticles", Phys. Rev. Lett. 38, 1440, 1977
- [51] P.W. Graham et al., "Experimental Searches for the Axion and Axion-like Particles", Annual Review of Nuclear and Particle Science 65, 2015 [arXiv: 1602.00039]
- [52] CAST collaboration, "New CAST limit on the axion-photon interaction", Nature Physics 13, pp. 584-590 (2017)
- [53] B. Penning, "The Pursuit of Dark Matter at Colliders - An Overview", 2017 [arXiv: 1712.01391]
- [54] M. Schumann, "Direct Detection of WIMP Dark Matter: Concepts and Status", J. Phys. G46 (2019) no.10, 103003 [arXiv: 1903.03026]
- [55] S.C. Martin et al., "The RAVE survey: constraining the local Galactic escape speed", Mon.Not.Roy.Astron.Soc.379:755-772, 2007
- [56] K. Freese, M. Lisanti, C. Savage, "Annual Modulation of Dark Matter: A Review", [arXiv: 1209.3339v3]
- [57] T.M. Undagoitia and L. Rauch, "Dark matter direct-detection experiments", J. Phys. G43 (2016) no.1, 013001 [arXiv: 1509.08767]
- [58] R. Bernabei et al., "First results from DAMA/LIBRA and the combined results with DAMA/NaI", Eur.Phys.J.C56:333-355, 2008 [arXiv: 0804.2741]
- [59] J.M. Gaskins, "A review of indirect searches for particle dark matter", Contemporary Physics, 2016 [arXiv: 1604.00014]
- [60] F.S. Queiroz, "Dark Matter Overview: Collider, Direct and Indirect Detection Searches", Max-Planck Institute of Physics
- [61] LAT collaboration, "Constraints on Dark Matter Annihilation in Clusters of Galaxies with the Fermi Large Area Telescope", JCAP 05(2010)025 [arXiv: 1002.2239]
- [62] A.A. Moiseev et al., "Dark Matter Search Perspectives with GAMMA-400", 2013 [arXiv: 1307.2345]
- [63] L. Covi et al., "Neutrino Signals from Dark Matter Decay", JCAP 1004:017, 2010 [arXiv: 0912.3521]
- [64] B. Lu and H. Zong, "Limits on the Dark Matter from AMS-02 antiproton and positron fraction data", Phys. Rev. D 93, 103517 (2016) [arXiv: 1510.04032]

- [65] J. Abdallah et al., "Simplified Models for Dark Matter Searches at the LHC", Phys. Dark Univ. 9-10 (2015) 8-23 [arXiv: 1506.03116]
- [66] H. An, L. Wang, H. Zhang, "Dark matter with t-channel mediator: a simple step beyond contact interaction", Phys. Rev. D 89, 115014 (2014) [arXiv: 1308.0592]
- [67] ATLAS Collaboration, "Search for dark matter and other new phenomena in events with an energetic jet and large missing transverse momentum using the ATLAS detector", JHEP 01 (2018) 126 [arXiv: 1711.03301]
- [68] CMS Collaboration, "Search for new physics in the monophoton final state in proton-proton collisions at $\sqrt{s} = 13$ TeV", J. High Energy Phys. 10 (2017) 073 [arXiv: 1706.03794]
- [69] CMS Collaboration, "Search for dark matter produced with an energetic jet or a hadronically decaying W or Z boson at $\sqrt{s} = 13$ TeV", JHEP 07 (2017) 014 [arXiv: 1703.01651]
- [70] CMS Collaboration, "Search for new physics in final states with an energetic jet or a hadronically decaying W or Z boson and transverse momentum imbalance at $\sqrt{s} = 13$ TeV", Phys. Rev. D 97, 092005 (2018) [arXiv: 1712.02345]
- [71] ATLAS Collaboration, "Search for dark matter in association with a Higgs boson decaying to two photons at $\sqrt{s} = 13$ TeV with the ATLAS detector", Phys. Rev. D 96 (2017) 112004 [arXiv: 1706.03948]
- [72] CMS Collaboration, "Search for associated production of dark matter with a Higgs boson decaying to $b\bar{b}$ or $\gamma\gamma$ at $\sqrt{s} = 13$ TeV", JHEP 10 (2017) 180 [arXiv: 1703.05236]
- [73] ATLAS Collaboration, "Search for new phenomena in dijet events using 37 fb⁻¹ of pp collision data collected at $\sqrt{s} = 13$ TeV with the ATLAS detector", Phys. Rev. D 96, 052004 (2017) [arXiv: 1703.09127]
- [74] CMS Collaboration, "Search for narrow and broad dijet resonances in proton-proton collisions at $\sqrt{s} = 13$ TeV and constraints on dark matter mediators and other new particles", JHEP 08 (2018) 130 [arXiv: 1806.00843]
- [75] C. Munoz, "Models of Supersymmetry for Dark Matter", FTUAM 17/2, IFT-UAM/CSIC-17-005, 2017 [arXiv: 1701.05259]
- [76] CMS Collaboration, "Searches for invisible decays of the Higgs boson in pp collisions at $\sqrt{s} = 7, 8, \text{ and } 13$ TeV", JHEP 02 (2017) 135 [arXiv: 1610.09218]
- [77] J. Alimena et al., "Searching for long-lived particles beyond the Standard Model at the Large Hadron Collider", 2019 [arXiv: 1903.04497]
- [78] A. Albert et al., "Recommendations of the LHC Dark Matter Working Group: Comparing LHC searches for heavy mediators of dark matter production in visible and invisible decay channels", 2017 [arXiv: 1703.05703]
- [79] M. Tanabashi et al., Particle Data Group, Phys. Rev. D 98, 030001 (2018)
- [80] R. Schicker, "The ALICE detector at LHC", 2005

- [81] LHCb Collaboration, "LHCb Detector Performance", *Int. J. Mod. Phys. A* 30, 1530022 (2015) [arXiv: 1412.6352]
- [82] J.T. Boyd, "LHC Run-2 and Future Prospects", 2020
- [83] E. Gschwendtner, "AWAKE, A Particle-driven Plasma Wakefield Acceleration Experiment", CERN Yellow Report CERN 2016-001, pp.271-288 [arXiv: 1705.10573]
- [84] M. Thomson, "Modern Particle Physics", Cambridge University Press, 2013
- [85] G. Apollinari et al., "High Luminosity Large Hadron Collider HL-LHC", CERN Yellow Report CERN-2015-005, pp.1-19 [arXiv: 1705.08830]
- [86] CMS Collaboration, "The CMS experiment at the CERN LHC", *JINST* 3 (2008) S08004
- [87] CMS Collaboration, "Precision measurement of the structure of the CMS inner tracking system using nuclear interactions", *JINST* 13 (2018) P10034 [arXiv: 1807.03289]
- [88] M.S. Kim, "CMS reconstruction improvement for the muon tracking by the RPC chambers", 2013 *JINST* 8 T03001 [arXiv: 1209.2646]
- [89] CMS Collaboration, "Performance of the CMS muon detector and muon reconstruction with proton-proton collisions at $\sqrt{s} = 13$ TeV", *JINST* 13 (2018) P06015 [arXiv: 1804.04528]
- [90] CMS Collaboration, "Particle-Flow Event Reconstruction in CMS and Performance for Jets, Taus, and MET", CMS-PAS-PFT-09-001, 2009
- [91] CMS Collaboration, "Description and performance of track and primary-vertex reconstruction with the CMS tracker", *JINST* 9 (2014) P10009 [arXiv: 1405.6569]
- [92] V. Knunz, "Measurement of Quarkonium Polarization to Probe QCD at the LHC", Springer theses, 2015
- [93] CMS Collaboration, "Performance of electron reconstruction and selection with the CMS detector in proton-proton collisions at $\sqrt{s} = 8$ TeV", *JINST* 10 (2015) P06005 [arXiv: 1502.02701]
- [94] J. Rembser, "CMS Electron and Photon Performance at 13 TeV", *J. Phys. Conf. Ser.* 1162 012008, 2019
- [95] P.L.S. Connor, "Review of jet reconstruction algorithms", Ryan Atkin *J. Phys. Conf. Ser.* 645 012008, 2015
- [96] CMS Collaboration, "Jet energy scale and resolution in the CMS experiment in pp collisions at 8 TeV", *JINST* 12 (2017) P02014 [arXiv: 1607.03663]
- [97] F. Beaudette, "The CMS Particle Flow Algorithm", 2014 [arXiv: 1401.8155]
- [98] CMS Collaboration, "Identification of heavy-flavour jets with the CMS detector in pp collisions at 13 TeV", *JINST* 13 (2018) P05011 [arXiv: 1712.07158]
- [99] CMS Collaboration, "Performance of missing transverse momentum reconstruction in proton-proton collisions at $\sqrt{s} = 13$ TeV using the CMS detector", *JINST* 14 (2019) P07004 [arXiv: 1903.06078]

- [100] L. Sonnenschein, "Analytical solution of ttbar dilepton equations", Phys.Rev.D73:054015, 2016
- [101] M.H. Seymour and M. Marx, "Monte Carlo Event Generators", MCnet-13-05, 2013 [arXiv:1304.6677]
- [102] B. Cabouat, J.R. Gaunt and K. Ostrolenk, "A Monte-Carlo Simulation of Double Parton Scattering", JHEP11(2019)061 [arXiv: 1906.04669]
- [103] R. Placakyte, "Parton Distribution Functions", 2011 [arXiv:1111.5452]
- [104] J. Alwall et al., "MadGraph 5 : Going Beyond", 2011 [arXiv:1106.0522]
- [105] C. Oleari, "The POWHEG-BOX", Nucl.Phys.Proc.Suppl.205-206:36-41 [arXiv:1007.3893]
- [106] S. Frixione et al., "The MC@NLO 4.0 Event Generator", CERN-TH/2010-216 [arXiv: 1010.0819]
- [107] B. Webber, "Parton shower Monte Carlo event generators", Scholarpedia
- [108] M. Bahr et al., "Herwig++ Physics and Manual", Eur.Phys.J.C58:639-707, 2008 [arXiv: 0803.0883]
- [109] T. Sjostrand, "A Brief Introduction to PYTHIA 8.1" Comput.Phys.Commun.178:852-867, 2008 [arXiv: 0710.3820]
- [110] A. Karneyeu et al., "MCPLOTS: a particle physics resource based on volunteer computing", European Physical Journal C 74 (2014) [arXiv: 1306.3436]
- [111] V. Lefebvre and S. Banerjee, "CMS Simulation Software Using Geant4", CMS-NOTE-1999-072, 1999
- [112] S. Banerjee, "Validation of Geant4 Physics Models Using Collision Data from the LHC", J. Phys.: Conf. Ser. 898 042005
- [113] A. Rizzi, G. Petrucciani and M. Peruzzi, "A further reduction in CMS event data for analysis: the NANO AOD format", J. Phys.: Conf. Ser. 214 06021
- [114] C.G. Lester and D.J. Summers, "Measuring masses of semi-invisibly decaying particles pair produced at hadron colliders", Phys.Lett.B463:99-103, 1999
- [115] K. Bloom, "CMS software and computing for LHC Run 2", ICHEP 2016 [arXiv: 1611.03215]
- [116] W. Tanenbaum, "A ROOT/IO Based Software Framework for CMS", ECONFC0303241:TUKT010, 2003
- [117] CMS Collaboration, "CMS Luminosity Measurements for the 2016 Data Taking Period", CMS-PAS-LUM-17-001, 2017
- [118] CMS Collaboration, "CMS Luminosity Measurements for the 2017 Data Taking Period", CMS-PAS-LUM-17-001, 2018
- [119] CMS Collaboration, "CMS Luminosity Measurements for the 2018 Data Taking Period", CMS-PAS-LUM-17-001, 2019
- [120] CMS Collaboration, "BRIL Work Suite"